A surface-anchored molecular four-level conductance switch based on single proton transfer

Willi Auwärter, Knud Seufert*, Felix Bischoff, David Ecija, Saranyan Vijayaraghavan, Sushobhan Joshi, Florian Klappenberger, Niveditha Samudrala, and Johannes V. Barth*

Physik Department E20, Technische Universität München, D-85748 Garching, Germany

The development of a variety of nanoscale applications[1, 2] requires the fabrication and control of atomic[3-5] or molecular switches[6, 7] that can be reversibly operated by light[8], a short range force[9, 10], electric current[11, 12] or some other external stimulus[13-15]. In order for such molecules to be used as electronic components, they should be directly coupled to a metallic support and the switching unit should be easily connectable to other molecular species without suppressing its switching performance. Here we show that a free-base tetraphenyl-porphyrin molecule, which is anchored to a silver surface, can function as a molecular conductance switch. The identified saddle-shaped conformer has two hydrogen atoms in its inner cavity that can be switched between two states with different local conductance levels using electrons from the tip of a scanning tunnelling microscope. Moreover, by selective deprotonation, a four-level conductance switch can be created. The resulting device, which could be controllably integrated into the surrounding nanoscale environment, relies on the transfer of a single proton and therefore contains the smallest possible atomistic switching unit.

Given their inherent functionality expressed in both biological and artificial systems[16], porphyrins and related compounds are well established molecular building blocks for surface based nanosystems. Their structural stability guarantees a straightforward sublimation in a highly controlled ultra-high vacuum environment and their chemical variability enables the self-assembly of well defined architectures as molecular films[17, 18], networks[19, 20], chains[21], multideckers[22] or metal-molecule contacts[23]. The tetrapyrrole macrocycle can host either a metal ion or two hydrogens. It is well established that the two central protons of a free-base porphyrin readily transfer between the two pairs of opposing nitrogens in the macrocycle (compare Fig. 1d and f) at ambient temperatures, the process being called tautomerization[24,

[25]. Recently, a pioneering study introduced a bi-stable conductance switch based on this mechanism relying on naphtalocyanine molecules on thin insulating films[12]. The two- and four-level conductance switches presented below also exploit a tautomerization reaction in individual molecules, but are directly anchored on a metallic support. To guarantee a stable read-out and a controlled operation, the molecular switches are studied by scanning tunnelling microscopy (STM) at low temperature, where the intrinsic proton transfer dynamics is suppressed.

STM offers unique opportunities to operate individual switches on the atomic scale[3]. Not only can the local atomic or molecular configurations be probed before and after flipping the switch, but the operation process itself can be followed by recording for example current traces as a function of time[26] and even be modified[27].

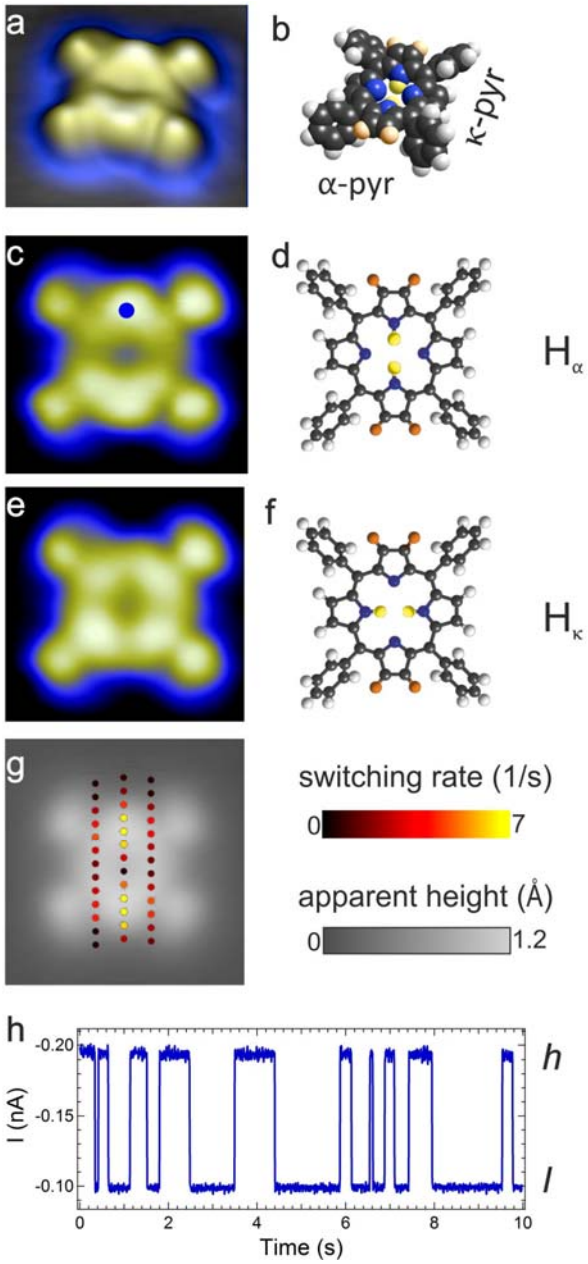

Figure 1 Double proton transfer in 2H-TPP/Ag(111). a, Pseudo 3D rendering of a high-resolution STM image of 2H-TPP/Ag(111). b, The corresponding model consistent with the NEXAFS data (c.f. Supplementary Information, Fig. S1) highlights the saddle-shape deformation resulting in two inequivalent pairs of pyrrole rings (α-pyr, marked in orange and κ-pyr) c, STM image of configuration H_α (I=0.1 nA, U=-0.2 V). d, Model highlighting the saddle-shape deformation and the position of the hydrogen pair in configuration H_α. e, STM image of configuration H_κ (I=0.1 nA, U=-0.2 V). f, Model of configuration H_κ. g, Spatial dependence of the switching rate displayed with colour-coded dots (recorded at -1.6 V and 2 nA). The highest rates (yellow markers) are observed above the α-pyr. h, Current versus time trace recorded -1.9 V at the position indicated in c. A switching between two current levels representing the high (*h*) and low (*l*) conductance states is clearly discernible.

Figure 1 introduces the 2H-TPP molecule hosting two hydrogen atoms in the inner cavity. At low temperatures they are localized at opposing nitrogens resulting in two possible *trans*-type configurations, represented by a 90° rotation of the hydrogen pair. The high-resolution STM images (Fig. 1a) combined with near-edge x-ray absorption spectroscopy data (Fig. S1, Supplementary Information) demonstrate that upon adsorption on the Ag(111) surface, the 2H-TPP adapts to a saddle-shaped macrocycle geometry with pairs of opposite pyrrole rings tilted upwards (α-pyr) or downwards (κ-pyr)[18, 28], respectively (Fig. 1b). This deformation is linked to rotated terminal phenyl rings by steric repulsion (Fig.1 and Fig. S1, Supplementary Information). Due to the resulting two-fold symmetric macrocycle geometry, the two positions of the hydrogen pair are not equivalent. The corresponding two configurations can be stably imaged and directly discriminated in high-resolution STM topographs taken at low bias voltages (Fig. 1 c and e). In configuration H_α, the hydrogen pair is aligned with the main axis of the molecule defined by the upward bent α-pyr rings (Fig. 1c and d), while in configuration H_κ, the hydrogen pair is positioned at the κ-pyr units (Fig. 1e and f). Applying a tunnelling current at a voltage exceeding a given threshold (vide infra) can result in a reversible switching between configuration H_α and H_κ that we attribute to an induced transfer of the proton pair. Other origins cannot explain the observed transformations: A conformational switching of the macrocycle would induce a rotation of the terminal phenyl legs. The high-resolution STM data, characterizing the orientation of the phenyl groups, show no difference related to the legs upon switching. Thus, a macrocycle adaptation is ruled out. In addition, deprotonation experiments (vide infra) clearly indicate that the positions of the inner hydrogens determine the two configurations H_α and H_κ. At low bias voltages, both configurations can be imaged stably, guaranteeing a reliable read-out of the switch. Throughout this letter, the wording hydrogen atom or pair is used to describe static configurations while dynamic processes are termed proton transfer.

The double proton transfer induced by applying a tunnelling current can be monitored directly by recording the tunnelling current *I* versus the time *t*. To this end, the tip is positioned over one of the α-pyr rings (cf. Fig. 1c), the tunnelling parameters (*I*, *U*) are set and the feedback loop is opened. The proton transfer can be triggered at any position above the molecule, however the rate is generally lower on the κ-pyr rings due to the two-fold macrocycle

symmetry (see Fig. 1g and Fig. S2, Supplementary Information) and drops to zero on the bare metal next to the molecule. A typical *I(t)* trace as displayed in Fig. 1 h clearly reveals a switching between two well-defined current levels. Hereby, the high conductance state *h* represents configuration H_α and the low conductance state *l* corresponds to configuration H_κ, as inferred from a comparison to the apparent heights of both pyrrole moieties in the STM images. Thus, 2H-TPP/Ag(111) represents a bi-stable system. A detailed discussion on the switching rate and the underlying mechanism follows below, however, it needs to be emphasized that we detected at most two current levels in all the data on 2H-TPP covering switching rates up to 0.5 kHz. Even after ordering 2H-TPP molecules in highly regular square arrays on Ag(111), the switching operation is conserved (cf. Fig. S3, Supplementary Information).

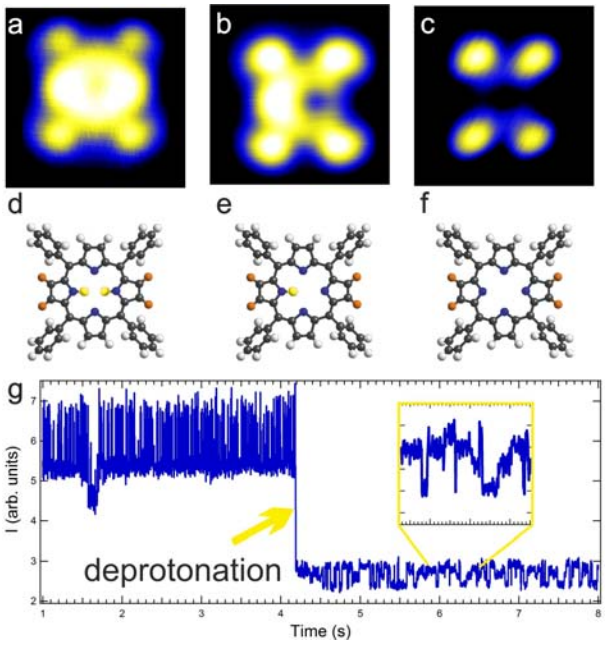

Figure 2 Sequential deprotonation of 2H-TPP/Ag(111). a, STM image of 2H-TPP (*I*=0.2 nA, U=-0.2 V). b, STM image of 1H-TPP. c, STM image of 0-TPP. d-f tentative models illustrating the 2H-TPP, singly deprotonated 1H-TPP and fully deprotonated 0H-TPP species. g, *I(t)* trace recorded at the center of 2H-TPP at 1.9 V. The sudden decrease in current represents the single deprotonation to 1H-TPP.

To upgrade this bi-stable system to a four-level conductance switch, we apply an atomically controlled deprotonation procedure: The STM tip is centered above the 2H-TPP macrocycle and a voltage pulse of typically 2 V is applied, resulting in the removal of one of the inner

protons. This single deprotonation process, yielding a 1H-TPP species, can be directly monitored in *I(t)* traces as shown in Fig. 2 g. Furthermore, a complete deprotonation of the macrocycle pocket can be achieved by a second step employing a voltage pulse of typically 2.2 V[29]. STM images representing all three species, i.e. 2H-TPP, 1H-TPP and 0H-TPP are shown in Fig. 2 a-c together with corresponding schematic models (Fig. 2 d-f). All these deprotonation events are irreversible. The deprotonated 0H-TPP is of no further interest, as the complete proton removal prevents any proton-related switching events, as confirmed experimentally. By contrast, the singly deprotonated 1H-TPP offers the possibility that the remaining hydrogen can be localized at each of the four nitrogen positions in the porphyrin pocket. Figure 3 presents all four configurations for the 1H-TPP molecule: $H_{\alpha 1}$, $H_{\kappa 1}$, $H_{\kappa 2}$ and $H_{\alpha 2}$. As in the 2H-TPP case, low-voltage imaging allows us to read out the position of the hydrogen, while higher voltages induce the switching that can be tracked via *I(t)* spectra. The trace in Fig. 2 g indicates that a switching can be observed even after the first deprotonation. Upon positioning the STM tip in a slightly asymmetric position above a pyrrole ring, up to four different current levels can be discriminated (Fig. 3 i and Fig. S5 in the Supplementary Information). In analogy to the 2H-TPP case, we relate these four conductance states to the position of the hydrogen in the porphyrin pocket (Fig. 3 e-g). We observe the highest conductance if the hydrogen is located at the κ-pyr where the tip is positioned. The two subjacent levels represent the positions on the two neighboring α-pyr rings and the lowest conduction level represents the opposing κ-pyr location, respectively, as confirmed experimentally. It should be noted that a suitable positioning of the tip is crucial to detect all four current levels: In case a sharp tip was perfectly centered above the macrocycle, only two current levels, representing the inequivalent pyrroles α-pyr and κ-pyr could be distinguished due to symmetry reasons.

The limited time resolution in the spectrum in Fig. 3 i suggests that the proton can not only be exchanged between neighboring nitrogens, but also be directly transferred to the opposing nitrogen, as indicated for example by the transition from the highest to the lowest conductance level observed at a time of 2.2 s. However, a careful analysis reveals that the transitions typically proceed via the intermediate levels. These experiments clearly indicate that the hydrogen position can be directly identified in constant current STM images. Vice

versa, a read out of a given current value unambiguously determines the configuration. However, it should be noticed that the observed protrusions do not represent the hydrogen itself, but rather the electronic effect reflecting its presence at the pyrrole rings of the porphyrin macrocycle. Applying a single switching event, the proton cannot be deliberately transferred to one specific position. However, this does not hamper the function of the switch: as the current levels which are recorded during operation of the switch are characteristic for the proton position and a feedback mechanism might be employed to freeze the desired state. In addition, there is some control on the switching direction: The residence time in the highest current state is shortest as clearly seen for example in Fig. S5 b. Thus we deal with a repulsive interaction where the proton residence time on the pyrrole close to the tip position is lower than on the other positions.

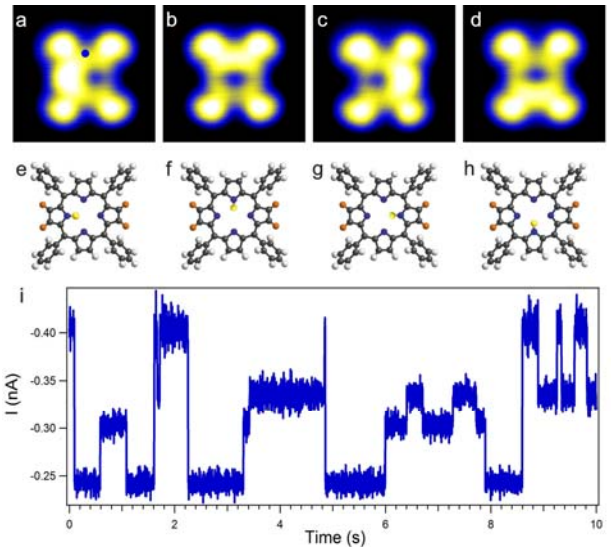

Figure 3 Visualization of the four proton positions in 1H-TPP/Ag(111). a-d, STM image of the very same 1H-TPP molecule in four configurations representing the hydrogen positions schematically shown in the corresponding models in e-f (*I*=0.2 nA, *U*=-0.2 V). i, current trace recorded in a slightly asymmetric position on an κ-pyr position (marked by the dot in a): The four conductance levels are clearly discernible (*I*=0.4 nA, *U*=-1.6 V).

To clarify the proton transfer mechanism, tens of thousands of switching events at different sample bias voltages *U* and tunnelling currents *I* were evaluated for both the 2H-TPP and 1H-TPP case. The analysis is summarized in Fig. 4 (current dependence) and Fig. 5 (voltage dependence). These plots rely on data recorded on an α-pyr position.

The linear current dependence of the switching rate S (Fig. 4) points to a one-electron process driving the proton transfer in 2H-TPP and 1H-TPP. This finding is corroborated by an analysis of the switching times presented in the Supplementary Information (Fig. S4). In combination with the voltage-dependent data presented below, we thus exclude the electric field between tip and molecule as dominating trigger for the tautomerization process. Nevertheless, as shown in the Supplementary Information (Fig. S6), the absolute switching rate depends on the termination of the STM tip and thus on the current density. A direct comparison of the switching rates between 2H-TPP and 1H-TPP was therefore performed with the same tip on the very same molecule prior and after deprotonation. The linear fits in Fig. 4 b reveal that the switching rate for 1H-TPP ($S_{1H\text{-}TPP}$, see Supplementary Information for a discussion of the data analysis, Fig. S7) and 2H-TPP ($S_{2H\text{-}TPP}$) are similar. However, the ratio $S_{1H\text{-}TPP} / S_{2H\text{-}TPP} = 1 \pm 0.4$ varies from molecule to molecule. This scatter might originate in minute modifications of the tip or subtle differences in the adsorption configuration during the deprotonation procedure and is beyond control in our experiments. Yet, importantly, the rate for 1H-TPP corresponds approximately to the rate for 2H-TPP at any given current value. Accordingly, in both cases a similar number of electrons is needed for one switching event, which points to an analogous process for switching in both species.

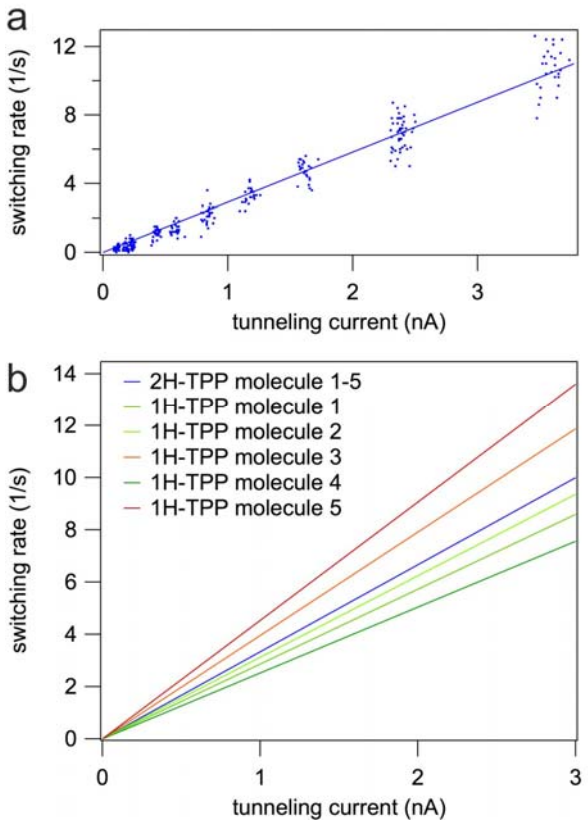

Figure 4 Current dependence of the switching rate *S* for 2H-TPP and 1H-TPP recorded on an α-pyr position. a, *S* increases linearly with tunnelling current *I*, pointing to a one electron process driving the proton transfer. Every single data point represents one *I(t)* spectrum where the current was averaged over the whole spectrum. The absolute rate depends on tip geometry (see Supplementary Information). The tip used for the experiment in panel a yields a rate $S_{2H\text{-}TPP}$ of 3.0 ± 0.1 $s^{-1}nA^{-1}$ at a constant voltage of -1.6 V. b, Comparison of *S* for 2H-TPP and 1H-TPP for five molecules. The blue line represents the normalized fits for the 2H-TPP species. The normalization to one average rate for 2H-TPP was performed to ease the comparison to 1H-TPP as the absolute rates for 2H-TPP vary from molecule to molecule. The green and red lines show the corresponding rates for the same molecules measured with an identical tip after the first deprotonation. While the rates are generally similar for 2H-TPP and 1H-TPP, the ratio $S_{1H\text{-}TPP}$ / $S_{2H\text{-}TPP}$ varies between 0.76 (dark green) and 1.36 (dark red).

Concerning the voltage dependence summarized in Fig. 5, for bias voltages below ± 0.5 V no switching events could be detected, confirming the stable read-out by STM images at low bias. Above this threshold, the switching rate *S* increases several orders of magnitude within 1 V for both 2H-TPP and 1H-TPP. In a small voltage range between ±1 and ±1.5 V the increase is nearly exponential and levels off at higher voltages[12]. Fig. 5a includes voltage dependent data recorded at three constant current values (0.5, 2, 4 nA, normalized to a rate of 1 at -1.5 V) that show an identical behaviour. The very similar rates for positive and negative sample bias voltages resulting in curves symmetric to the Fermi level (Fig. 5a)

exclude an exclusive role of one specific molecular orbital in the proton transfer. Indeed, tunnelling spectra recorded above an α-pyr show a highly asymmetric local electronic density of states around the Fermi level (Fig. 5b). This is of importance, as recent theoretical models addressing surface-anchored switches based on tautomerization consider solely an electron transfer via the lowest unoccupied molecular orbital (LUMO)[30, 31]. The voltage threshold and symmetry agreeing for both polarities rather points to an excitation of the proton transfer by electrons tunnelling inelastically through the porphyrin. Indeed, it is generally agreed that the proton transfer in free-base porphyrins involves both vibrational excitations in the macrocycle that temporarily reduce the separation of the hydrogen from an adjacent nitrogen site and proton tunnelling. The corresponding barrier heights, determined by theoretical and experimental studies, range from 0.5 to 0.6 eV [29,31-33] and thus coincide with the onset voltage observed in our experiments. Overall, the peculiar voltage dependence of the switching rate calls for thorough theoretical studies.

Adjusting *I* and *U*, *S* can be easily tuned from 0 to approximately 500 Hz reaching quantum yields (events per electron) of about $7 \cdot 10^{-7}$ (Fig. S8, Supplementary Information). The limitations in switching frequency are given by both the voltage threshold for deprotonation and lateral displacements of the molecule induced at high currents.

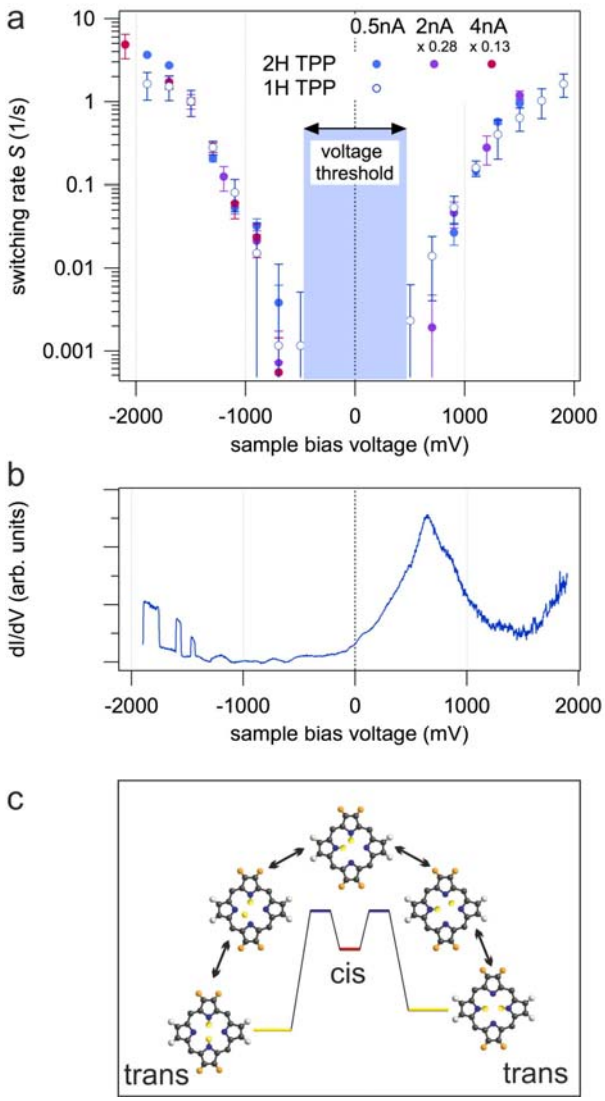

Figure 5 Voltage dependence of the switching rate *S* for 2H-TPP and 1H-TPP excited on an α-pyr position. a, The voltage dependences measured at a constant current of 0.5, 2 and 4 nA, respectively, show a threshold for switching of about 500 mV followed by a sharp increase with similar slope for both polarities (All data points were normalized to 1 at -1.5 V using scaling factors of 0.28 and 0.13 respectively). b, Characteristic scanning tunnelling spectra recorded above an α-pyr position of 2H-TPP representing the local density of states (LDOS) that is clearly asymmetric for both polarities. The broad feature around 700 mV is identified as the LUMO, while no occupied resonance is observed at negative bias voltages. The discontinuities observed at elevated voltages of both polarities are effects of the proton transfer. c, Scheme sketching the stepwise proton transfer via a *cis*-like intermediate state for 2H-TPP (the phenyl groups are omitted for clarity; see text for discussion). The macrocycle deformation upon adsorption potentially lifts the degeneracy of both *trans*-configurations.

The obvious similarity between 2H-TPP and 1H-TPP in both, the current and voltage dependence, suggests that the same process is involved in the switching. This is in full agreement with most current studies agreeing that the double proton migration in liquid and solid state proceeds in a stepwise, asynchronous manner involving an intermediate state[32,34,

[35]. The scheme in Fig. 5c sketches this reaction pathway. Instead of an immediate, synchronous migration of both protons, they are transferred one by one. The intermediate state is characterized by a *cis*-type configuration where the two hydrogens occupy neighboring nitrogen sites. Judging from literature, the *cis*-state has a very short lifetime[32,35] and relaxes either back to the initial state or to the final rotated configuration (Fig. 5c). Hence, the *cis*-state decays immediately on the time scale of a typical STM experiment and is not detectable. Accordingly, from a practical point of view the 2H-TPP/Ag(111) indeed constitutes a two-level conductance switch and recent theoretical suggestions claiming four conductance levels detectable by STM in a related system seem rather optimistic[31]. Assuming that the switching process is triggered by a direct excitation of hydrogens by tunnelling electrons, the observed similarities between 2H-TPP and 1H-TPP indicate that in both cases one proton is transferred to an adjacent nitrogen site for each excitation. This interpretation substantiates the idea that also for a metal surface-anchored porphyrin, the tautomerization reaction proceeds in an asynchronous way. If, on the other hand, the switching originates in a deformation of the macrocycle induced by tunnelling electrons and the resulting proton transfer is not the rate limiting process, an immediate or asynchronous motion can not be discriminated.

In summary, we introduced a novel metal-anchored four-level conductance switch based on prototropy. Specifically, an individual proton is reversibly transferred in a singly deprotonated 1H-TPP molecule. Thus, we provided a demonstration for the smallest possible atomistic switching unit. The direct comparison to 2H-TPP/Ag(111) representing a bi-stable system with two well-defined conductance levels allows us to gain insight on the proton transfer mechanism the switches base on: The data point to a one-electron induced excitation as trigger for the proton migration in both species and suggest an identical switching process in both 1H-TPP and 2H-TPP. As the periphery of the molecule is not affected by the proton migration in the inner pocket, the switch is integrable into nanoscale architectures. During the operation of the switch, the STM tip is stationary and only plays the role of the second electrode. Consequently, solely an appropriate electrode and no complete STM setup is needed for the switching action. All the above features make the free-base TPP species presented here ideal candidates for future nanoscale applications, especially as our findings

might be easily extended to the huge class of other free-base porphyrins as well as related macrocyclic compounds.

Methods

All experiments were performed in a custom designed ultra-high vacuum chamber housing a commercial scanning tunnelling microcscope (STM) operated at 6 K (www.lt-stm.com). The base pressure during the experiments was below 2×10^{-10} mbar. Repeated cycles of Ar^+ sputtering and annealing to 725 K were used to prepare the Ag(111) single crystal. Subsequently 2H-TPP molecules (Sigma Aldrich, purity ≥ 99 %) were dosed from a thoroughly degassed quartz crucible held at 600 K. During deposition the sample temperature was kept at room temperature to grow 2H-TPP arrays or at 150 K to get individual 2H-TPP molecules. All STM images were recorded in constant current mode using an electrochemically etched tungsten tip prepared by sputtering and controlled dipping into the Ag(111) substrate. In the figure captions *U* refers to the bias voltage applied to the sample. The WsXM program (www.nanotec.es) was used to display the STM images. The current traces *I(t)* were recorded at constant height (open feedback loop) after setting the desired parameters (*I*, *U*).

Acknowledgements

The authors thank J. Repp for helpful suggestions concerning the data analysis. Work supported by the ERC Advanced Grant MolArt (n° 247299), TUM-IAS and the Munich Center for Advanced Photonics (MAP). N.S. acknowledges a scholarship from DAAD. D.E. thanks the European Commission for support through the Marie Curie IntraEuropean Fellowship for Career Development FP7 program.

Author contributions

K.S., W.A., F.B., D.E., S.V., S.J., and N.S. performed the STM experiments, analyzed and interpreted the experimental data. F.K. supported the data analysis and contributed the NEXAFS experiments. W.A. K.S. and J.V.B conceived the studies and co-wrote the paper.

Additional Information

Supplementary information accompanies this paper at

www.nature.com/naturenanotechnology. Reprints and permission information is available

online at http://npg.nature.com/reprintsandpermissions/.

Correspondence and requests for materials should be addressed to W.A.

1. Browne, W. R. & Feringa, B. L. Making molecular machines work. Nature Nanotechnology 1 25-35 (2006).
2. Balzani, V., Credi, A. & Venturi, M. Molecular machines working on surfaces. ChemPhysChem 9, 202-220 (2008).
3. Eigler, D. M., Lutz, C. P. & Rudge, W. E. An atomic switch realized with the scanning tunnelling microscope. Nature 352, 600-603 (1991).
4. Repp, J., Meyer, G., Olsson, F. E. & Persson, M. Controlling the Charge State of Individual Gold Adatoms. Science 305, 493-495 (2004).
5. Quaade, U. J., Stokbro, K., Thirstrup, C. & Grey, F. Mechanism of single atom switch on silicon. Surf. Sci. 415, L1037-1045 (1998).
6. Donhauser, Z. J. et al. Conductance Switching in Single Molecules Through Conformational Changes. Science 292, 2303-2307 (2001).
7. Iancu, V. & Hla, S.-W. Realization of a four-step molecular switch in scanning tunneling microscope manipulation of single chlorophyll-a molecules. PNAS 103, 13718-13721 (2006).
8. Wolf, M. & Tegeder, P. Reversible molecular switching at a metal surface: A case study of tetra-tert-butyl-azobenzene on Au(111). Surf. Sci. 603, 1506-1517 (2009).
9. Loppacher, C. et al. Direct determination of the energy required to operate a single molecule switch. Phys. Rev. Lett. 90, 066107 (2003).
10. Moresco, F. et al. Conformational Changes of Single Molecules Induced by Scanning Tunneling Microscopy Manipulation: A Route to Molecular Switching. Phys. Rev. Lett. 86, 672-675 (2001).
11. Henzl, J., Mehlhorn, M., Gawronski, H., Rieder, K.-H. & Morgenstern, K. Reversible cis-trans Isomerization of a Single Azobenzene Molecule. Angew. Chem. Int. Ed. 45, 603-606 (2006).
12. Liljeroth, L., Repp, J. & Meyer, G. Current-Induced Hydrogen Tautomerization and Conductance Switching of Naphtalocyanine Molecules. Science 317, 1203-1206 (2007).
13. Pivetta, M., Ternes, M., Patthey, F. & Schneider, W.-D. Diatomic Molecular Switches to Enable the Observation of Very-Low-Energy Vibrations. Phys. Rev. Lett. 99 (2007).
14. Wäckerlin, C. et al. Controlling spins in adsorbed molecules by a chemical switch. Nature Communications 1057 (2010).
15. Qiu, X. H., Nazin, G. V. & Ho, W. Mechanisms of Reversible Conformational Transition in a Single Molecule. Phys. Rev. Lett. 93, 196806 (2004).
16. Dolphin, D. (ed.) The Porphyrins (Academic, New York, 1978).

17. Scudiero, L., Barlow, D. E. & Hipps, K. W. Physical Properties and Metal Ion Specific Scanning Tunneling Microscopy Images of Metal(II) Tetraphenylporphyrins Deposited from Vapor onto Gold (111). J. Phys. Chem. B 104, 11899-11905 (2000).
18. Auwärter, W. et al. Site-specific electronic and geometric interface structure of Co-tetraphenyl-porphyrin layers on Ag(111) Phys. Rev. B 81, 245403 (2010).
19. Spillmann, H. et al. A two-dimensional porphyrin-based porous network featuring communicating cavities for the templated complexation of fullerenes. Adv. Mater. 18, 275-279 (2006).
20. Écija, D. et al. Hierarchic Self-Assembly of Nanoporous Chiral Networks with Conformationally Flexible Porphyrins. ACS Nano 4, 4936-4942 (2010).
21. Heim, D. et al. Self-Assembly of Flexible One-Dimensional Coordination Polymers on Metal Surfaces. J. Am. Chem. Soc. 132, 6783-6790 (2010).
22. Écija, D. et al. Assembly and Manipulation of Rotatable Cerium Porphyrinato Sandwich Complexes on a Surface. Angew. Chem. Int. Ed. 50, 3872-3877 (2011).
23. Nazin, G. V., Qiu, X. H. & W.Ho. Visualization and spectroscopy of a metal-molecule-metal bridge. Science, 77-81 (2003).
24. Hennig, J. & Limbach, H.-H. Kinetic Study of Hydrogen Tunnelling in meso-Tetraphenylporphine by Nuclear Magnetic Resonance Lineshape Analysis and Selective T1ρ-Relaxation Time Measurements. J. Chem. Soc., Faraday Trans. 2 75, 752-766 (1979).
25. Butenhoff, T. J. & Moore, C. B. Hydrogen Atom Tunneling in the Thermal Tautomerism of Porphine Imbedded in a n-Hexane Matrix. J. Am. Chem. Soc. 110, 8336-8341 (1988).
26. Lastapis, M. et al. Picometer-Scale Electronic Control of Molecular Dynamics Inside a Single Molecule. Science 308, 1000-1003 (2005).
27. Martin, M. et al. Mastering the Molecular Dynamics of a Bistable Molecule by Single Atom Manipulation. Phys. Rev. Lett. 97, 216103 (2006).
28. Seufert, K. et al. Cis-dicarbonyl binding at cobalt and iron porphyrins with saddle-shape conformation. Nature Chemistry (2011).
29. Sperl, A., Kröger, J. & Berndt, R. Controlled Metalation of a Single Adsorbed Phthalocyanine. Angew. Chem. Int. Ed. 50, 5294-5297 (2011).
30. Sarhan, A., Arboleda Jr, N. B., David, M., Nakanishi, H. & Kasai, H. STM-induced switching of the hydrogen molecule in naphtalocyanine. J. Phys.: Condens. Matter 21, 064201 (2009).
31. Fu, Q., Yang, J. & Luo, Y. Mechanism for tautomerization induced conductance switching of naphthalocyanin molecule. Appl. Phys. Lett. 95, 182103 (2009).
32. Baker, J., Kozlowski, P. M., Jarzecki, A. A. & Pulay, P. The inner-hydrogen migration in free base porphyrin. Theor. Chem. Acc. 97, 59-66 (1997).
33. Braun, J., Hasenfratz, C., Schwesinger, R. & Limbach, H.-H. Free Acid Porphyrin and Its Conjugated Monoanion. Angew. Chem. Int. Ed. 33, 2215-2217 (1994).
34. Ghosh, A. First-Principles Quantum Chemical Studies of Porphyrins. Acc. Chem. Res. 31, 189-196 (1998).
35. Maity, D. K., Bell, R. L. & Truong, T. N. Mechanism and Quantum Mechanical Tunneling Effect on Inner Hydrogen Atom Transfer in Free Base

Porphyrin: A Direct ab Initio Dynamics Study. J. Am. Chem. Soc. 122, 897-906 (2000).